DEFORMATION EXTRACTION AND ANALYSIS OF COSEISMIC DEFORMATION FIELD BASED ON D-INSAR TECHNOLOGY

Anping Shi[1] , Lin Jiang[2], Lv Zhou[1,3,*], Hao Tang [1], Bangding Wei[1], Jiahao Li[1]

1 Guilin University of Technology, Guilin, China
2 Guangxi Polytechnic of Construction, Nanning, China
3 Guangxi Key Laboratory of Spatial Information and Geomatics, Guilin University of Technology, Guilin, China

Commission III, WG III/IVa

KEY WORDS: Sentinel-1A, Differential Interferometric Synthetic Aperture Radar, Dual polarization mode, Coseismic deformation field, Yulin earthquake.

ABSTRACT:

Extracting the seismic deformation field and analyzing the surface deformation after an earthquake occurs are of great significance for explaining earthquake mechanism and earthquake relief. Through the dual polarization mode of the two-pass method D-InSAR technology, this paper extracted the coseismic deformation fields based on two Sentinel-1A SAR images covering the Yulin earthquake area, and analyzed the surface deformation. The results show that the subsidence area obtained by VV and VH polarization modes are consistent. The uplift center areas are located in Tongxin Village in Rong County and Mapo Town in Luchuan County, and the subsidence center area is located in Fuxin Town of Beiliu City in the northeast. In the earthquake area, the maximum uplift derived by the VV mode SAR data is 12.1 cm, and the maximum subsidence is 5.8 cm. the maximum uplift obtained by the VH mode SAR data is 11.2 cm, and the maximum subsidence is 9 cm. The results obtained by the two polarization modes are consistent. D-InSAR technology can accurately obtain the coseismic deformation field, which provides data guarantee for the follow-up study of the inversion of seismic source parameters in the region.

1. INTRODUCTION

An earthquake is a natural movement phenomenon of the earth's crust, which releases huge amounts of energy and produces seismic waves in the process. In addition to causing extremely serious casualties, earthquakes can also cause secondary disasters such as tsunamis, mountain landslides, and collapse of the earth's surface. Therefore, monitoring the surface deformation of related seismic zones has very important practical research significance. The traditional monitoring modes mainly include: GNSS (Global Navigation Satellite System), geodetic leveling, triangulation and automatic laser ranging, but these modes are not suitable for large-area deformation monitoring in cities, mountainous areas, etc. Interferometric Synthetic Aperture Radar (InSAR), as a non-contact measurement mode, has the advantages of all-weather, large area, and low cost (Liu et al. 2010), and has become a large-scale landslide monitoring (Wang et al. 2010), snow depth inversion (Liu et al. 2014) and important monitoring methods such as surface deformation. Differential Interferometric Synthetic Aperture Radar (D-InSAR) is developed on basis of InSAR. The principle is to obtain effective surface deformation information through differential interferometry for two SAR images covering the same area before and after deformation (Zbeker et al. 1994). D-InSAR technology can be used to monitor the earth's surface deformation at the centimeter level or millimeter level (Hao et al. 2009; Burgman et al. 2000). D-InSAR has attracted more and more attention in the research fields of crustal movement, focal mechanism, volcanic eruption, land subsidence and glacier movement, and its technical application is becoming more and more mature. Massonnet et al. (1993) obtained the coseismic displacement field of the 1992 Landers earthquake in California based on the SAR data of ERS-1. The acquired deformation map is roughly the same as the GPS monitoring data. Researchers (Pritchard et al. 2002; Lasserre et al. 2005) concluded through experiments that the differential interferometric radar technology based on C-band SAR data is feasible for monitoring surface deformation in dry areas. Zhang et al. (2000) extracted the seismic coseismic displacement field in Zhangbei area by using ERS-1/2 interferometric image pair, which further confirmed the potential of D-InSAR technology in seismic monitoring and research. Zang et al. (2017) studied earthquake deformation in L'Aquila, Italy by using the two-pass method, and successfully obtained the displacement of coseismic displacement field in the Light of Sight (LOS) direction of radar. Zhang et al. (2012) applied D-InSAR technology to obtain the surface deformation in Yushu earthquake area, and analyzed the focal mechanism and seismogenic mechanism of the earthquake. Shan et al. (2002) successfully extracted the vertical crustal deformation field by using InSAR technology. Sun et al. (2008) observation and analysis of the deformation field of Wenchuan Ms8.0 earthquake in 2008. Gudmundsson et al. (2002) studied the three-dimensional deformation field of Reykjanes Peninsula in Iceland by using the D-InSAR data and GPS deformation data of ERS-1 / 2. In synthesizing GPS and InSAR Data to obtain the three-dimensional seismic deformation, they used the new optimization methods of Markov random-field regularization and a simulated annealing algorithm. D-InSAR technology has great potential in the future seismic monitoring research and monitoring because of the ease of interference image acquisition and the simplicity of displacement field acquisition algorithm.

The Yulin earthquake occurred in a mountainous area with rugged terrain and dense vegetation, which brings great difficulties to conventional measurement methods such as leveling and GPS. D-InSAR technology does not need to go to the field measurement and can obtain a wide range of detection information, so it has great advantages in data acquisition. In this paper, the deformation information of Yulin earthquake area in Guangxi is extracted by differential interferometric radar

* Corresponding author

technology, and then the results of coseismic deformation field in the earthquake area are analyzed. Different from other seismic research using a single polarization mode, the deformation field of two polarization modes is compared in this paper.

2. STUDY REGIONS AND DATA SOURCES

The study area is Liujing Town, Beiliu City, Yulin, China, with the longitude and latitude of the focal center at 22.18° N and 110.51° E. A 5.2 magnitude earthquake occurred here at 22:55 on October 12, 2019. The focal center was at the junction of Guangdong and Guangxi, and the focal depth was up to 10km. The 5.2 magnitude quake was the largest of 12 earthquakes that have struck the area in recent years. Guangxi is not an earthquake prone region, but the Yulin region experienced a 5.2 magnitude earthquake in 2019. Therefore, it is very important to use D-InSAR technology for seismic research in Guangxi region. The study area is shown in Figure 1:

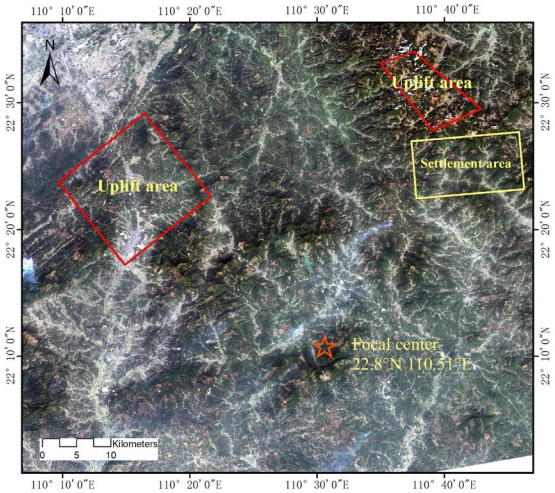

Figure 1. Overview of earthquakes in Yulin study area

The experimental image data used in this paper were Sentinel-1A SAR images provided by ESA and SRTM DEM released by NASA. The data of two scenes in Yulin area of Guangxi before and after the earthquake were selected, and the two scene images were used for differential interference processing. Specific parameters of Sentinel-1A data are illustrated in table 1:

Area	Time	Satellite type	Rail type	Band	Polarization mode
Yulin	10.9、10.21	Sentinel-1A	Drop rail	C	VV、VH

Table 1. Satellite data related parameters

3. THE PRINCIPLE OF D-INSAR

D-InSAR technology is a technique for obtaining deformation information of monitored targets through two or more interferometric measurements. The interference phase obtained based on differential interferometry can be expressed as (Yang et al. 2015).

$$\phi_{\text{int}} = \phi_{\text{def}} + \phi_{\text{topo}} + \phi_{\text{atm}} + \phi_{\text{flat}} + \phi_{\text{noise}} \quad (1)$$

Where ϕ_{def} represents the deformation phase of the radar line of sight; ϕ_{topo} is the phase resulting from changes in surface elevation; ϕ_{flat} denotes the phase caused by the earth's reference ellipsoid. ϕ_{atm} is the phase produced by atmospheric effects. ϕ_{noise} stands for noise.

In order to obtain deformation phase ϕ_{def}, topographic phase ϕ_{topo} of equation (1) needs to be removed. D-InSAR technology is divided into two-pass method (Li et al., 2008), three track mode and four track mode according to the different modes adopted to remove terrain phase. The following is a comparative analysis of the advantages and disadvantages of the three technical methods. The DEM of two-pass method is external download, which has the advantage of simple processing steps, but the disadvantage is that it is difficult to configure the interference image and reference DEM accurately. Different from two-pass method, there-pass method generates DEM in the measurement process and does not require image pre-registration before differential measurement, which is its biggest advantage. The disadvantage is that the coherence of SAR image of there-pass method is not high. Four-pass method generates DEM in the measurement process, which has the advantages of large amount of data and low selection difficulty. The disadvantage is that a large number of SAR images make it difficult to register.

The two-pass method firstly generates the interference map reflecting the topographic information by simulating the external DEM data. Then the phase information of deformation is extracted by differential interferometry. Figure 2 shows the geometric relationship of D-InSAR in the two-pass method.

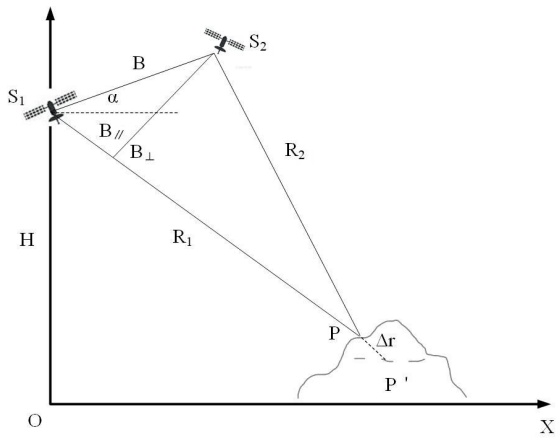

Figure 2. Schematic diagram of D-InSAR

After removing ϕ_{topo}, ϕ_{flat}, ϕ_{atm} and ϕ_{noise} in Equation (1), the deformation phase can be obtained:

$$\phi_{\text{def}} = \frac{4\pi}{\lambda}\Delta r \quad (2)$$

In equation (2), Δr is the shape variable of radar line of sight. According to equation (2), the form variable can be expressed as:

$$\Delta r = \frac{\lambda}{4\pi}\phi_{def} \quad (3)$$

In this paper, two-pass method and external DEM mode were used for experiment. A group of SAR images before and after the Yulin earthquake were selected for phase differential

processing. Then the interference phase was obtained. Orbital parameters were used to remove the phase of the reference ellipsoid and the topographic phase was calculated using an external DEM. After subtracting the topographic phase from the total interference phase, the deformed differential interference phase was obtained, and finally get the deformed phase.
The flow chart of the two-pass method is as follows:

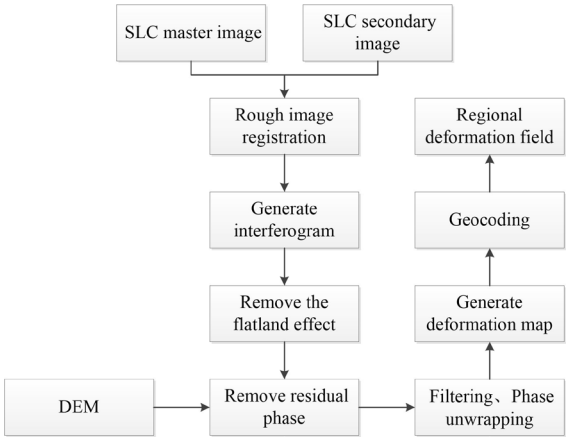

Figure 3 Flow chart of two-pass method

4. DATA PROCESSING AND RESULT ANALYSIS

4.1 Extraction of coseismic deformation field

The key steps for Sentinel-1A data processing are as follows:
First, the two images are registered based on the orbital information. Then the interferogram can be obtained by multiplying the complex conjugate of SLC data. The interferogram obtained at this time contains the flatland effect. Therefore, it is necessary to remove the flatland effect based on precise orbit data combined with DEM data. Finally, the interferogram removing the flatland effect is obtained.

4.1.1 Baseline estimation

An important step before differential interferometry is to make a baseline estimate of two scenes. The ultimate purpose of baseline estimation is to reflect the quality of interferometric images. Interference must occur under two conditions: one is that two or more antennas overlap in the ground reflection obtained, and the other is that the vertical baseline cannot exceed the critical value. In addition, baseline parameters also affect elevation accuracy, and even affect the linkage "slope" effect in DEM. Therefore, it is particularly important to use appropriate methods to estimate the parameters of the baseline. In this paper, the original image data of two scenes in Yulin are processed, and the baseline processing results are as follows: The space baseline is 15.276m, far less than the critical baseline 5031m, which meets the interference conditions. The 2π change of each phase represents a deformation of 0.028m with a time baseline of 12 days.

4.1.2 Generated interferogram

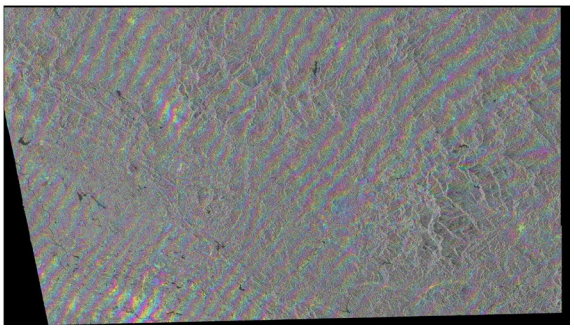

Figure 4. Interference diagram

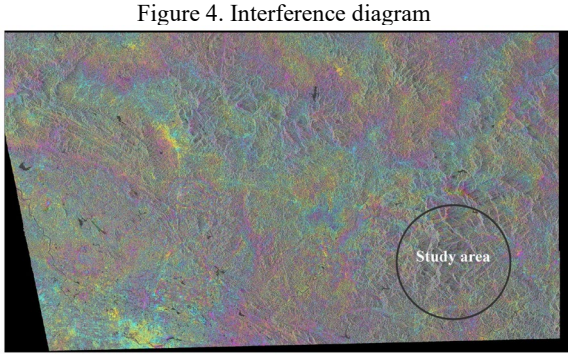

Figure 5. Interference diagram after flattening

As can be seen from the interferogram after flattening in figure 5, the fringe distinctiveness in the study area is stronger than that in other areas. Through the following steps, the hidden information in the fringe and the surface deformation information can be obtained.

4.1.3 Filtering and generating coherence coefficient

The interferogram generated in the previous step contains a lot of noise, which will affect the efficiency and accuracy of phase unwrapping. Common filtering methods are shown in Table 2:

Filtering method	Characteristic
Adaptive	It is reliable for high-resolution data
Boxcar	The optimal filter depends on the frequency of local interference fringes
Goldstein	The influence of spatial and temporal baseline noise is reduced by improving the interference fringes of the image.

Table 2 Three common filtering methods

In this paper, Goldstein filter mode is selected to remove noise error (Sun et al. 2013). Compared with other filtering modes, this mode can not only improve the signal-to-noise ratio of interferogram, but also reduce the incoherence noise caused by baseline. Then take VV polarization mode as an example to analyze Yulin image. The interferogram and coherence diagram after filtering are shown in Figure 6; Figure 7:

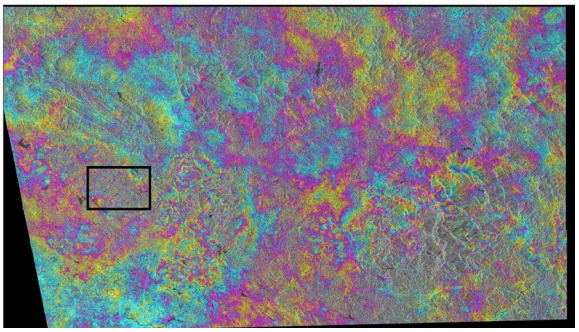

Figure 6. Interferogram after filtering

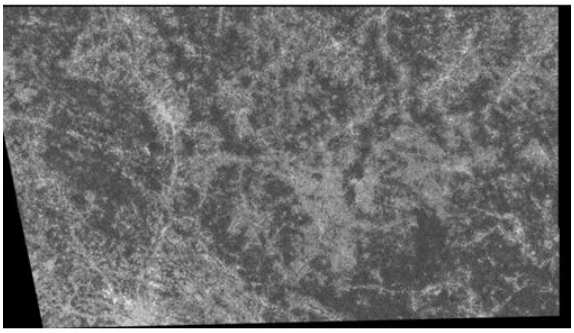

Figure 7. Coherence coefficient diagram

After filtering, it can be seen intuitively that the black box in the interferogram is decoherent after the earthquake compared with that before the earthquake, which confirms the occurrence of the earthquake. Figure 7 shows that the coherence coefficient is large. Because the coherence coefficient is judged according to the color depth, the lighter the color, the higher the coherence of the matching degree of the two scenes.

4.1.4 Phase unwrapping

The essence of phase unwrapping is the process of recovering the whole phase period. After phase unwrapping, the linear change of terrain can be well matched to solve the whole cycle ambiguity. In this paper, the minimum cost flow (MCF) mode was used for unwrapping. Its advantage is that all pixels can be considered, especially in the region with a large range of low coherence. The images of Yulin in VV polarization mode were analyzed. The phase unwrapping result is shown in Figure 8:

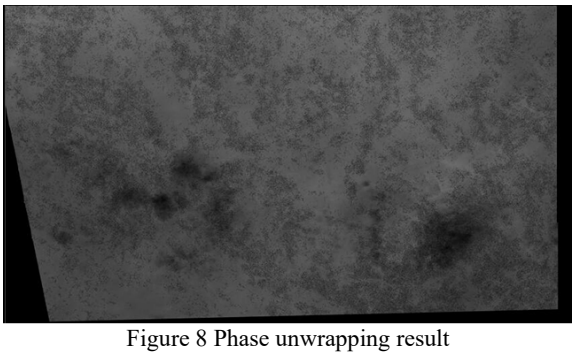

Figure 8 Phase unwrapping result

4.1.5 Geocoding

Geocoding is the last step in differential interference processing. The products obtained by differential interferometry through a series of technical processes are completed in the radar coordinate system and cannot be used directly. In order to facilitate interpretation and understanding, the product needs to be geocoded into the geographic coordinate system. Geocoding can correct geometric deformation of SAR image caused by terrain relief. The deformation map of radar Line of Sight (LOS) surface is obtained by geocoding. In this paper, the shape variable in the vertical direction needs to be transformed. Yulin images in VV polarization mode were analyzed, and the results are shown in Figure 9:

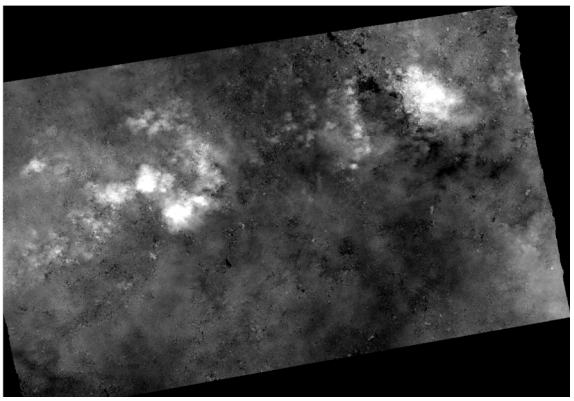

Figure 9 Result after geocoding

4.2 Result analysis

Based on Sentinel-1A images, D-InSAR technology was used to extract the co-seismic deformation field of the Yulin earthquake. The range, spatial and temporal distribution of deformation field and deformation size were analyzed. This provided a reference for seismic decision making and earthquake risk assessment.

4.2.1 Space distribution

In this paper, VV polarization mode (The signal is transmitted vertically and received vertically) and VH polarization mode (Signal is transmitted vertically and received horizontally) were used for data processing. The deformation characteristics of Yulin earthquake region under VV and VH modes were analyzed. The analysis was conducted at the focal center (22.18°N, 110.51°E). It can be seen from the VV monitoring diagram of Yulin earthquake surface deformation in Figure 10. There was a slight subsidence around the focal center, and the main deformation areas were distributed in the northeast and northwest directions of the focal center. From the surface deformation monitoring map of Yulin earthquake in VV polarization mode in figure 10, it can be seen that there was a relatively slight settlement around the focal center, and the main deformation areas were distributed in the northeast and northwest of the focal center. In figure 10, obvious uplift occurs in the red area box in the northeast (The center of the uplifting area was Tongxin Village, Rong County) and in the red area box in the northwest (Lifting center is Mapo Town, Luchuan County). The uplift deformation area expands outward, and the value of deformation decreases gradually. However, the northeast yellow area (subsidence center was Fuxin Town, Beiliu City) had a certain degree of subsidence phenomenon. The settlement deformation area expands outward, the deformation value gradually decreases, and the seismic deformation field area is asymmetrically distributed. As can be seen in figure 6, there is incoherence in the area in the black box. There were two main reasons. One was the dense vegetation and complex landform in the earthquake area. In the process of radar signal reflection, the moisture existing in the vegetation will increase the absorption rate of the vegetation to the radar signal, and then affect the signal reflectivity. When the radar works, the incoherence phenomenon occurs when the reflected signal is not received. Second, the ground deformation caused by earthquake was too large, which will also lead to incoherence.

4.2.2 Magnitude

Under VV polarization mode, the maximum uplift of the deformation area is about 12.1 cm and the maximum settlement is about 5.8 cm. Under VH polarization mode, the maximum uplift of the deformation area is about 11.2 cm and the maximum settlement is about 9 cm.

4.2.3 Comparison of VV and VH polarization modes

By comparing the results of the two polarization modes, the monitoring results of VH mode and VV mode were roughly the same, and the surface deformation regions of Yulin earthquake obtained by the two polarization modes were highly consistent.

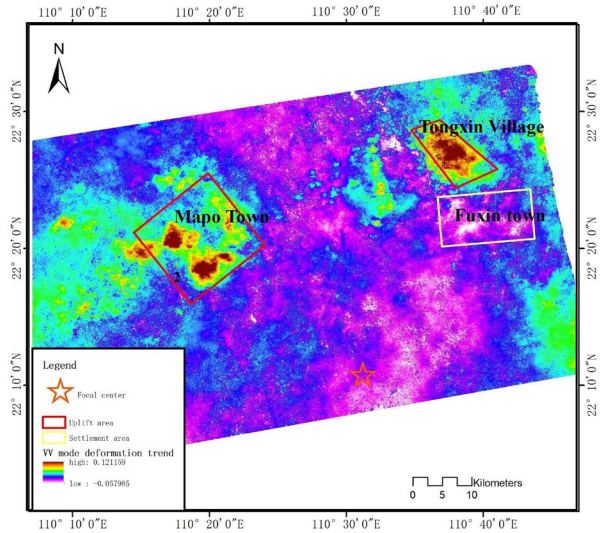

Figure 10 Surface deformation monitoring chart of Yulin earthquake in VV mode

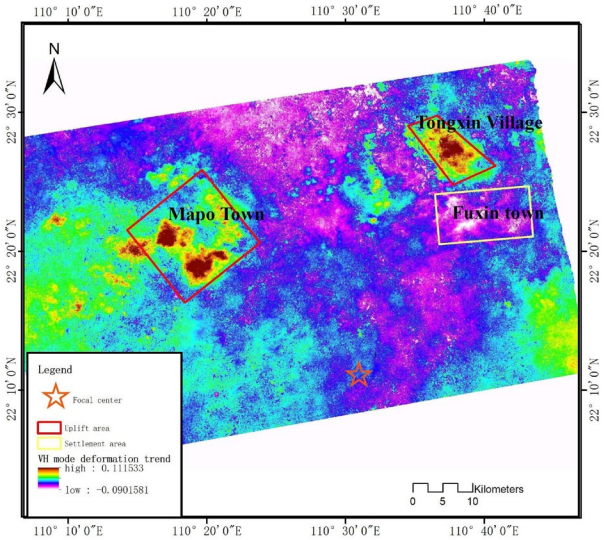

Figure 11 Surface deformation monitoring chart of Yulin earthquake in VH mode

5. CONCLUSION

This paper used Sentinel-1A SAR images to extract surface deformation in Yulin earthquake area based on D-InSAR technology. After obtaining the coseismic deformation field, the trend of surface deformation was analyzed. Finally, the range of subsidence area and deformation value caused by earthquake were determined. The results show that: 1) In Yulin Area, the maximum uplift is 12.1 cm and the maximum settlement is 5.8 cm under VV mode, and the maximum uplift is 11.2 cm and the maximum settlement is 9 cm under VH mode. 2) For the Yulin earthquake, both VV and VH polarization modes can reverse the surface deformation results with high accuracy. 3) D-InSAR technology can accurately detect the surface variables after earthquake, obtain the coseismic deformation field, and provide scientific data support for post-earthquake mechanism research, earthquake relief and other aspects.

ACKNOWLEDGEMENTS

This work was supported by Guangxi Universities Young and Middle-aged Teachers' Basic Scientific Research Ability Improvement Project (Grant No. 2020KY06032), the Guangxi Science and Technology Plan Project (Grant No. GUIKE AD19110107), the Natural Science Foundation of Guangxi (Grant No. 2018GXNSFBA050006), the National Natural Science Foundation of China (Grant No. 42064003).
The authors wish to thank ESA for freely providing Sentinel-1A data through Sentinels Scientific Data Hub, and NASA for providing the DEM data.

REFERENCES

Burgman R., Rosen P.A., Fielding E.J., et al. 2000. Synthetic aperture radar interferometry to measure Earth's surface topography an its deformation. *Annual Review of Earth and Planetary Sciences*, 28: 169-209.

Gudmundsson S, Gudmundsson M.T., Bjornsson H., et al. 2002. Three-dimensional glacier surface motion maps at the Gjalp eruption site, Iceland inferred from combining InSAR and other ice-displacement data. *Annals of Glaciology*, 34(01): 315-322.

Hao K.X., Si H., et al. 2009. Coseismic surface-ruptures and crustal deformations of the 2008 Wenchuan earthquake Mw7.9. *China Geophysical Research Letters*, 36(11): 192-200.

Li Y., Liu L.T., Xue H.P., et al. 2008. Study on deformation field of Bam earthquake by D-InSAR. *Geodesy and geodynamics*, (01): 32-35.

Li H., Xiao P.F., Feng X.Z., et al. 2014. Snow depth inversion method based on heavy rail InSAR. *Glacial permafrost*, 36(03): 517-526.

Lasserre C., Peltzer G., Cramp E., et al. 2005. Coseismic deformation of the 2001 Mw=7.8Kokoxili earthquake in Tibet, measured by synthetic aperture radar interferometry. *Joural of Geophysical Research*. 110(B12408).

Liu Y.H., Qu C.Y., Shan X.J., et al. 2010. Application of SAR remote sensing image in Wenchuan earthquake disaster identification. *Journal of Seismology*, 32(02): 214-223.

Massonnet D., Rossi M., Carmona C., et al. 1993. The dis-placement field of the landers earthquake mapped by radar interferometry. *Nature*. 364(6433): 138-142.

Pritchard M.E., Simons M., Rosen P.A., et al. 2002. Hensley Sand Webb E H. Coseismic slip from the 1995 July 30 Mw=8.1 Antofagasta, Chile, earthquake as constrained by InSAR and GPS observations. *Geophys J Int*. 150: 362-376.

Sun Q., Li Z.W., Zhu J.L., et al. 2013. Improved Goldstein filter for InSAR noise reduction based on local SNR. *Journal of Central South University*, 20(07): 1896-1903.

Sun J.B., Liang F., Shen Z.K., et al. 2008. Wenchuan MS8 InSAR deformation observation and preliminary analysis of 0 earthquake. *Seismogeology*, 30(03): 789-795.

Shan X.J., Ma J., Song X.Y., et al. 2002. Study on focal rupture characteristics of Zhangbei Shangyi earthquake by using surface deformation field obtained by spaceborne D-InSAR Technology. *China Earthquake*. 18(02): 119-126.

Wang G.J., Xie M.W., Qiu C., et al. 2010. Application of D-InSAR technology in large-scale landslide monitoring. *Geotechnical Mechanics*, 31(04): 1337-1344.

Yang J.K., Fan H.D., Zhao W.Y., et al. 2015. Monitoring and prediction of mining subsidence based on D-InSAR technology and grey Verhulst model. *Metal mine*, (03): 143－147.

Zhang R., Liu G.X., Yu B., et al. 2012. Extraction of coseismic surface deformation field of Yushu earthquake by radar differential interferometry based on alos PALSAR data. *Science of Surveying and Mapping*, 37(04): 13-16.

Zang Q.B., Huang T., Guo X.T., et al. 2017. Study on Coseismic Deformation of L'Aquila, Italy based on D-InSAR Technology. *Journal of Henan University of Technology* (*NATURAL SCIENCE EDITION*), 36(01): 52-57.

Zhang H., Wang C., Liu Z., et al. 2000. Differential interferometry technique for obtaining coseismic deformation field of Zhangbei earthquake. *Chinese Journal of image and graphics*, 2000(06): 52-55.

Zbeker H.A., Rosen P., et al. 1994. On the derivation of coseismic displacement fields using differential radar interferometry. *The Landers earthquake*. 99(B10).